

Spike sorting: What is it? Why do we
need it? Where does it come from? How
is it done? How to interpret it?

I. What is spike sorting, neurophysiological
origin of the recorded signal and short
history of the field.

Christophe Pouzat

Mathématiques Appliquées à Paris 5 (MAP5)

Université Paris-Descartes and CNRS UMR 8145

christophe.pouzat@parisdescartes.fr

Where are we ?

Ensemble recordings

What is spike sorting?

What do we measure?

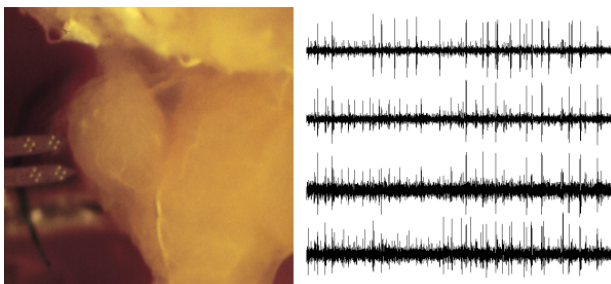
A short history of spike sorting

Why do we want to record from many neurons?

Neurophysiologists are trying to record many neurons at once
with single neuron resolution because:

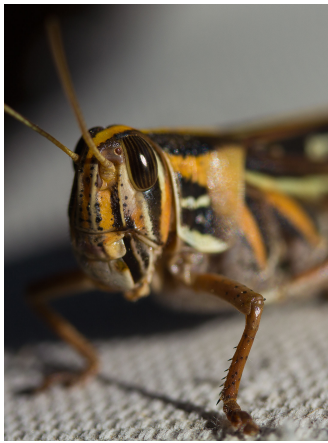
- ▶ They can collect more data per experiment.
- ▶ They have reasons to think that neuronal information processing might involve synchronization among neurons, an hypothesis dubbed **binding by synchronization** in the field.

Ensemble recordings: multi-electrode array (MEA)



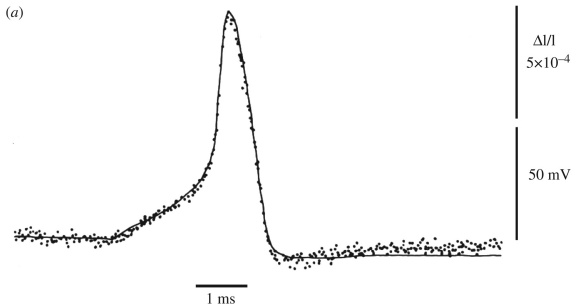
Left, the brain and the recording probe with 16 electrodes (bright spots). Width of one probe shank: $80 \mu m$. Right, 1 sec of raw data from 4 electrodes. The local extrema are the action potentials. The insect shown on the figure is a locust, *Schistocerca americana*. Source: Pouzat, Mazor and Laurent.

What a *Schistocerca americana* looks like?

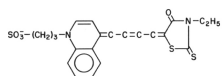


"Schistocerca americana headshot" by Rob Ireton - <http://www.flickr.com/photos/24483890@N00/7182552776/>.
Licensed under Creative Commons.

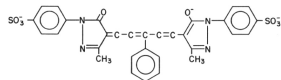
Voltage sensitive dyes



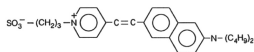
(b)



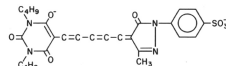
XVII, merocyanine, absorption, birefringence



RH155, oxonol, absorption



di-4-ANEPPS, styryl, fluorescence

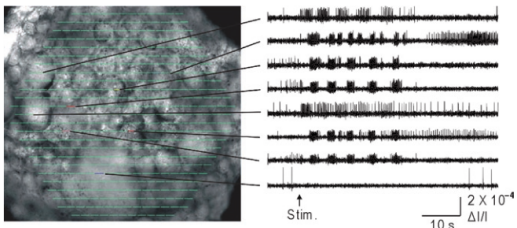


XXV, oxonol, fluorescence, absorption

Fig. 2 of Homma et al (2009) *Phil Trans R Soc B* 364:2453.

Ensemble recordings: voltage-sensitive dyes (VSD)

FIGURE 5.3. Superimposing an image of the preparation with the diode array makes it easy to inspect the firing of different neurons. The *left panel* shows an image of the dorsal surface of the pedal ganglion, superimposed in Neuroplex with a display of the 464 acquired optical traces in their corresponding diode positions (green lines). The *right panel* shows how clicking on diodes of interest displays their optical data. These are filtered, unaveraged recordings from single diodes, each showing the firing recorded from the indicated ganglion location. A five cycle swim motor program was elicited by a 10 Hz, 1 s, 10 V stimulus to Pedal Nerve 3, delivered at the arrow.



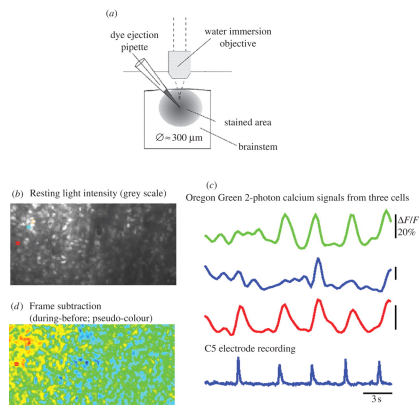
Imaging of the pedal ganglion of *Tritonia* by Frost et al (2010), Chap. 5 of *Membrane Potential Imaging in the Nervous System*, edited by M. Canepari and D. Zevecic.

What a *Tritonia* looks like?



"Tritonia festiva" by Daniel Hershman from Federal Way, US - edmonds4. Licensed under Creative Commons Attribution 2.0 via Wikimedia Commons.

Ensemble recordings: calcium concentration imaging



Embryonic mouse brainstem-spinal chord preparation. Fig. 10 of Homma et al (2010) *Phil Trans R Soc B* 364:2453.

Where are we ?

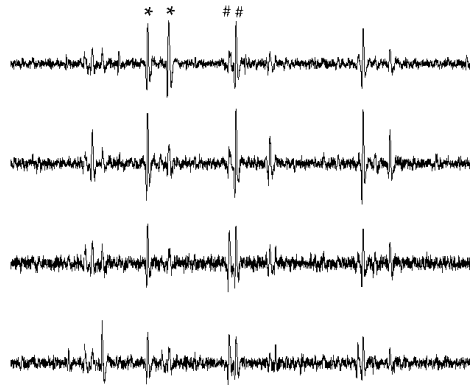
Ensemble recordings

What is spike sorting?

What do we measure?

A short history of spike sorting

Why are tetrodes used?



The last 200 ms of the locust figure. With the upper recording site only it would be difficult to properly classify the two first large spikes (**). With the lower site only it would be difficult to properly classify the two spikes labeled by ##.

What do we want?

- ▶ Find the number of neurons contributing to the data.
- ▶ Find the value of a set of parameters characterizing the signal generated by each neuron (e.g., the spike waveform of each neuron on each recording site).
- ▶ Acknowledging the classification ambiguity which can arise from waveform similarity and/or signal corruption due to noise, the probability for each neuron to have generated each event (spike) in the data set.
- ▶ A method as automatic as possible.

A similar problem (1)

- ▶ Think of a room with many people seating and talking to each other using a language we do not know.
- ▶ Assume that microphones were placed in the room and that their recordings are given to us.
- ▶ Our task is to isolate the discourse of each person.

A similar problem (2)



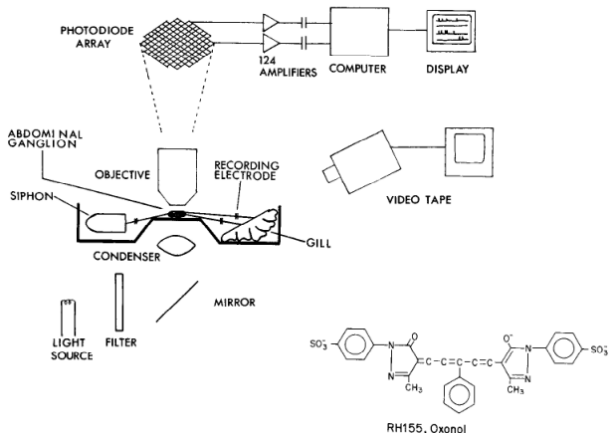
With apologies to Brueghel (original, without microphones, in Vienna, Kunsthistorisches Museum).

A similar problem (3)

To fulfill our task we could make use of the following features:

- ▶ Some people have a low pitch voice while other have a high pitch one.
- ▶ Some people speak loudly while other do not.
- ▶ One person can be close to one microphone and far from another such that its talk is simultaneously recorded by the two with different amplitudes.
- ▶ Some people speak all the time while other just utter a comment here and there, that is, the discourse statistics changes from person to person.

VSD does not eliminate the sorting problem (1)



VSD recording from Aplysia's abdominal ganglion, Fig. 1 of Zecevic et al (1989) *J Neurosci* 9:3681.

Aplysia



Source: Wikipedia, Licensed under Creative Commons Attribution-Share Alike 3.0 via Wikimedia Commons.

VSD does not eliminate the sorting problem (2)

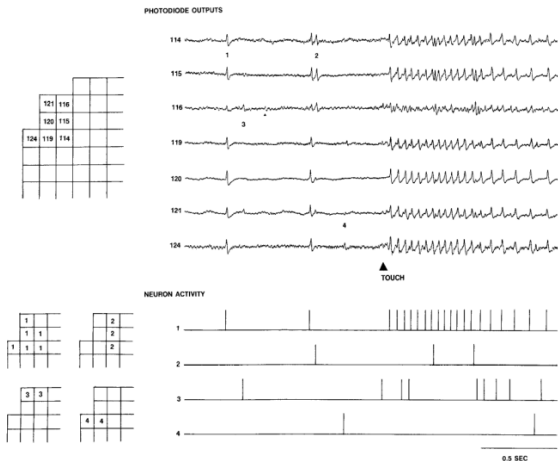


Fig. 2 of Zecevic et al (1989).

Calcium signals have slow kinetics!

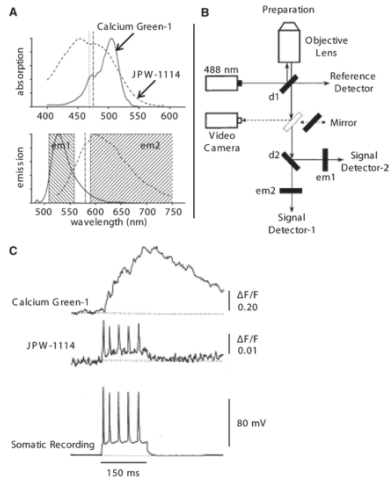
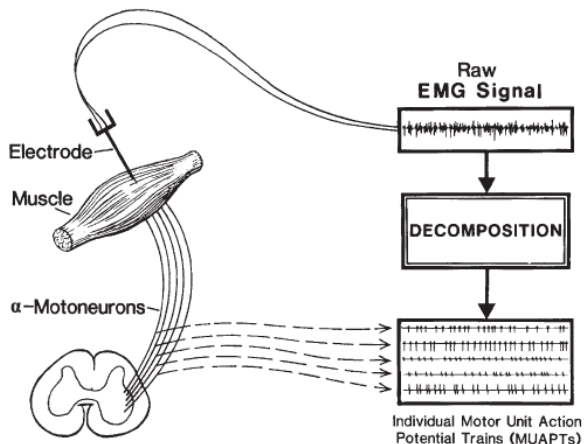


FIGURE 4.3. Combining voltage and calcium imaging using JPW-1114 and Calcium Green-1. (A) Combined excitation and emission spectra of JPW-1114 (dotted line) and Calcium Green-1 (straight line) with the relative placement of the emission filters em1 and em2. (B) Epifluorescence configuration for high-speed random-access, laser-scanning microscopy (similar to the configuration reported in Fig. 4.1b). (C) Representative voltage and calcium signals simultaneously recorded from the proximal dendrite of a cultured hippocampal pyramidal neuron; action potentials were elicited by current injection through a somatic patch pipette also used for somatic recording. Reproduced from Bullen and Saggau (1998) with the permission of Springer.

Fig. 4 of Canepari et al (2010), Chap. 4 of *Membrane Potential Imaging in the Nervous System*, edited by M. Canepari and D. Zevecic.

Spike sorting also matters for neurologists



Neurologist perform daily electromyographic (EMG) recordings monitoring **muscle fibers** action potentials.

Where are we ?

Ensemble recordings

What is spike sorting?

What do we measure?

A short history of spike sorting

Membrane potential: intracellular and extracellular ionic concentrations

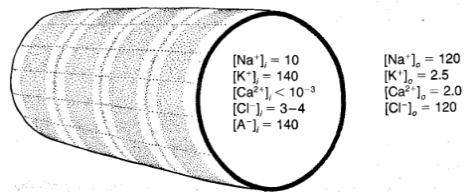


Figure 4-13 Concentrations of common ions are very different inside and outside a vertebrate skeletal muscle cell. The concentrations shown are in millimoles per liter. The concentration given for intracellular Ca^{2+} is for the free, unbound, and unsequestered ion in the myoplasm. Because the list of ions is incomplete, the totals do not balance out perfectly. $[A^-]_i$ represents the molar equivalent negative charges carried by various impermeant anions.

Fig. 4-13 of Randall et al (1997) *Eckert Animal Physiology* W H Freeman and Company.

Different concentrations and selective permeability generate membrane potential

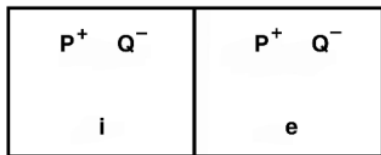


Figure 3.2. Concentration Cell. The concentration cell has a calibrated membrane area separating two compartments, designated i and e . Known ionic concentrations are present in each compartment. Here two hypothetical ions, P^+ and Q^- , are present in each compartment. The compartments are well mixed, so that concentration differences within a compartment are insignificant. The concentration cell provides well-defined geometry within which concentration changes over time can be examined.

Fig. 3.2 of Plonsey and Barr (2007) *Bioelectricity. A quantitative Approach*. Springer.

The equilibrium potential (when a single ion is membrane permeable, here ion P) is given by the **Nernst equation**:

$$V_m^{eq} = \Phi_i - \Phi_e = \frac{-RT}{Z_p F} \ln \left(\frac{[C_p]_i}{[C_p]_e} \right).$$

Nernst equilibrium potential

Table 3.1. Ionic Concentrations^a

	Muscle (frog)		Nerve (squid axon)	
	Intracellular mM	Extracellular mM	Intracellular mM	Extracellular mM
K ⁺	124.0	2.2	397	20
Na ⁺	4.0	109.0	50	437
Cl ⁻	1.5	77.0	40	556
A ⁻	126.5			

^aThe A⁻ ion is large and impermeable.

Table 3.3. Faraday's Constant F and the Gas Constant R

Constant	Value
F	96,487 Coulombs/mole
R	8.314 Joules/degree K-mole
RT/F	8.314 × .300/96487 = 25.8 mV at 27 °C

Tables 3.1 and 3.3 of Plonsey and Barr (2007).
We get for the potassium ion in the squid:
 $-25.8 \times \ln 397/20 = -78 \text{ mV}.$

A Model of a membrane "patch"

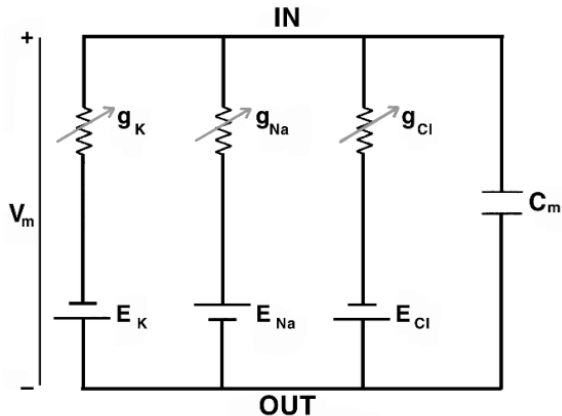
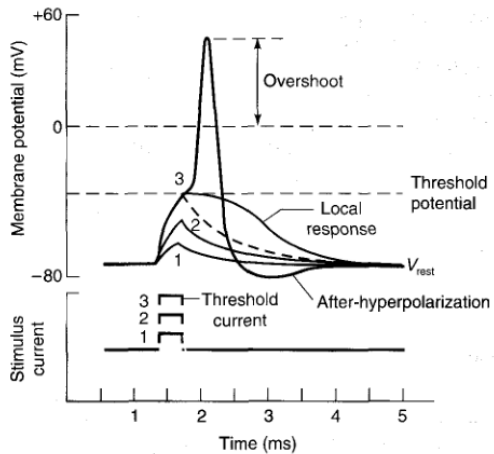


Figure 3.3. The Parallel-Conductance Model of an Excitable Membrane (IN = intracellular, OUT = extracellular). Independent conductance channels are present for K^+ , Na^+ , and Cl^- . Transmembrane potential V_m is positive when the inside has higher potential than the outside. The battery polarity is chosen to show that usually the Nernst potentials of E_K and E_{Cl^-} are negative (inside more negative than outside) and that of E_{Na} is positive (inside more positive than outside).

Fig. 3.3 of Plonsey and Barr (2007).

What makes (most) neurons "special"?



If we *depolarize* neurons "enough", an "active response" of *action potential* is generated. Fig. 5-16 of Randall et al (1997).

Conductance changes are responsible for the action potential

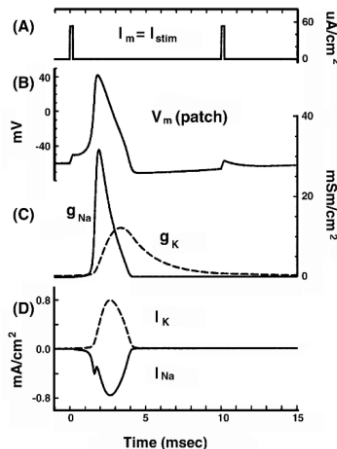
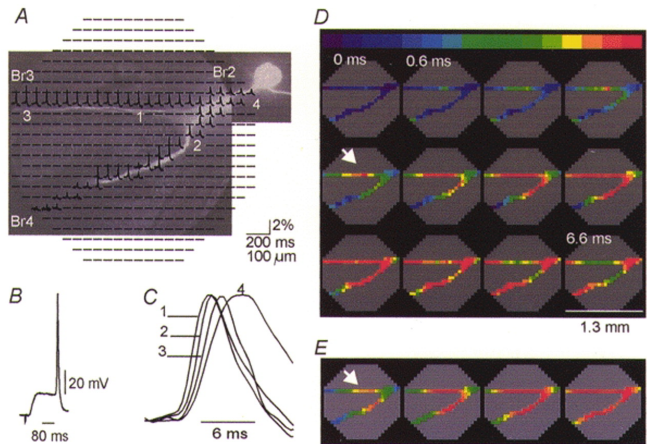


Figure 5.16. Membrane Potential and Currents following Stimulus. The stimulus is at the top (A). Below it are the calculated changes in membrane potential (B), sodium and potassium conductances (C), and sodium and potassium currents (D). All curves are for a squid giant axon membrane patch. The second stimulus is seen to elicit essentially no response even though it is of the same size and duration as the first (for which an action potential results, as is seen). It therefore identifies the condition as refractory. Since a larger stimulus would generate an action potential, this is a *relatively refractory period*. The stimulus amplitude is $53 \mu\text{A}/\text{cm}^2$, and its duration is 0.2 msec. The second stimulus is similar in amplitude and duration and occurs after a delay of 15 msec. The resting potential is -60 mV while $T = 6.3^\circ\text{C}$. Calculations were based on the Hodgkin-Huxley equations.

Fig. 5.16 of Plonsey and Barr (2007).

The action potential propagates!



VSD recording from the giant metacerebral neuron of *Helix aspersa*. Fig. 2 of Antic et al (2000) *J Physiol* 527:55.

The giant metacerebral neuron of *Helix aspersa*

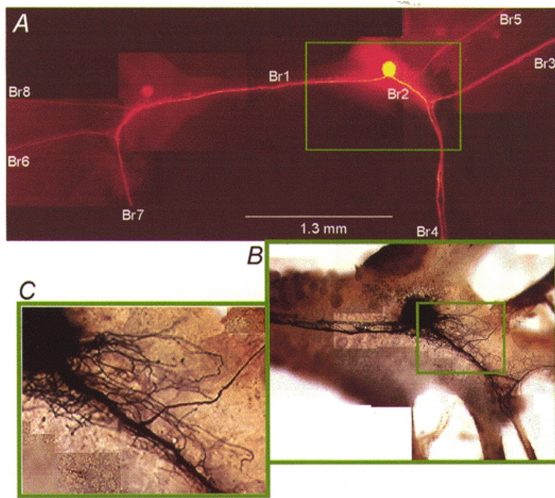


Fig. 1 of Antic et al (2000).

Helix aspersa



"Snail1web". Licensed under Public domain via Wikimedia Commons.

Currents associated with a non-uniform membrane potential

When the membrane potential, V_m , is spatially non-uniform axial, I_i [A], and trans-membrane, i_m [A/L], currents are necessarily present:

$$I_i = -\pi a^2 \sigma_i \partial V_m / \partial x$$

and

$$i_m = \pi a^2 \sigma_i \partial^2 V_m / \partial x^2 ,$$

where a is the axon / neurite diameter, the neurite is assumed to "seat" on the x axis, an axial current is positive if it goes in the increasing x direction and a trans-mambrane current is positive if it goes from inside to outside and σ_i is the intracellular conductance per centimeter [S/L]. See for instance Plonsey and Barr (2007) Chap. 6 and 8.

Currents associated with a propagating AP

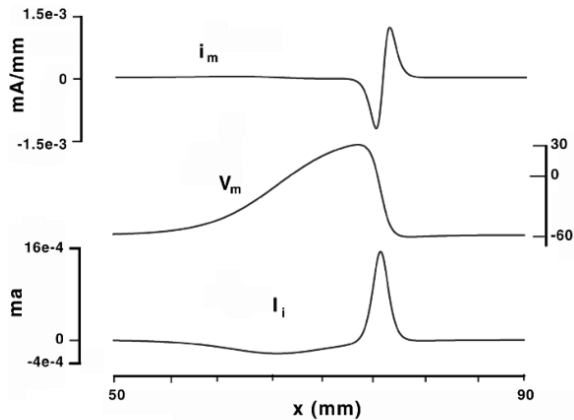


Figure 8.3. Transmembrane Potential V_m , Intracellular Current I_i , and Transmembrane Current i_m . The Figure shows a transmembrane potential (middle). Other traces give the transmembrane (top) and intracellular axial (bottom) currents, as determined from the transmembrane potential using Eqs. (8.7) and (8.8).

Fig. 8.3 of Plonsey and Barr (2007).

Extracellular potential associated with a current source (1)

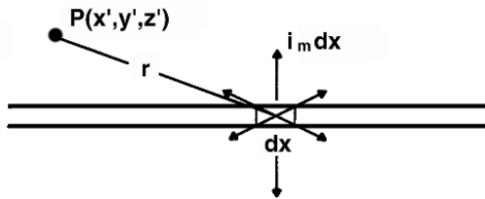
For a point current source of intensity I_0 in a medium of conductivity per unit length σ_e , the extracellular potential (with respect to a reference at infinity) depends only on the distance, r , to the source and is given by:

$$\Phi_e = \frac{1}{4\pi\sigma_e} \frac{I_0}{r}.$$

For a fiber "seating" on the x axis we get at a point (x', y', z') the potential:

$$\Phi_e(x', y', z') = \frac{1}{4\pi\sigma_e} \int_L \frac{i_m(x)}{\sqrt{(x - x')^2 + y'^2 + z'^2}} dx.$$

Extracellular potential associated with a current source (2)



Part of Fig. 8.5 of Plonsey and Barr (2007).

Using our previous expression for i_m we get:

$$\Phi_e(x', y', z') = \frac{a^2 \sigma_i}{4\sigma_e} \int_L \frac{\partial^2 V_m(x)}{\partial x^2} \frac{dx}{\sqrt{(x - x')^2 + y'^2 + z'^2}}.$$

Notice the dependence on the fiber cross-section.

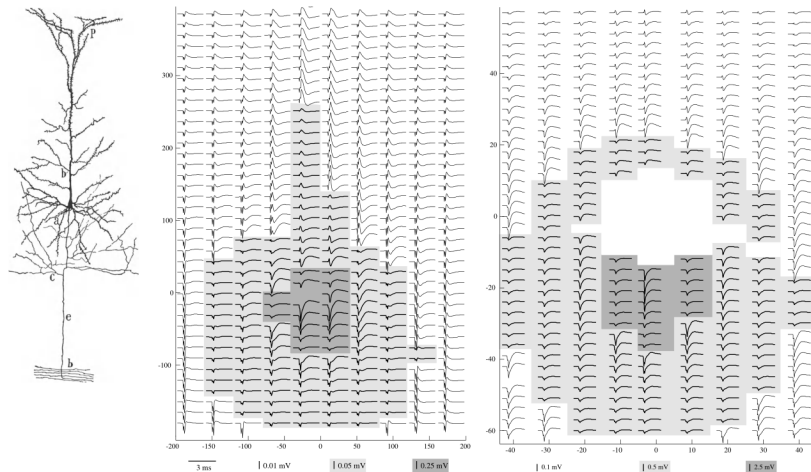
Observed extracellular potential

FIG. 16. Summary of the results of recording the response of single motoneurones, intra- and extracellularly, showing structures within and near which it is presumed the different forms of potential are recorded. Note that baseline for tracings of potential indicates position with respect to distorted drawing of a motoneurone on left; it does not give correct relative distances between recording positions at which such potentials were obtained. See text for full discussion.



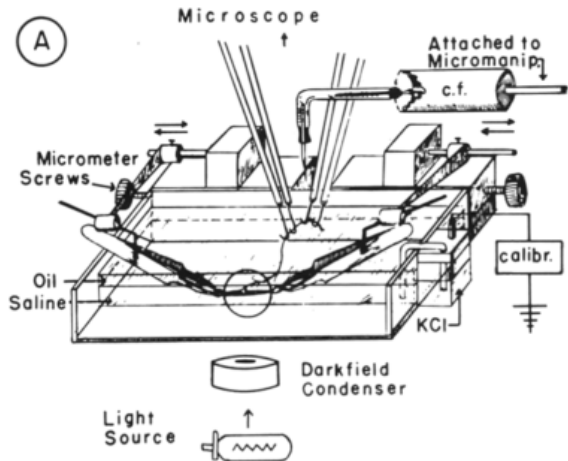
Fig. 16 of Fatt (1957) *J Neurophys* 20:27. Recordings from Cats motoneurons.

Computed extracellular potential



Left, Fig. 8 of Santiago Ramón y Cajal (1899), middle and right Fig. 2.4 and 2.5 of Holt PhD thesis (Caltech, 1999).

The stretch receptor of *Homarus americanus* (1)



The preparation, Fig. 1 A of Eyzaguirre and Kuffler (1955a) J Gen Phys 39:87.

The stretch receptor of *Homarus americanus* (2)

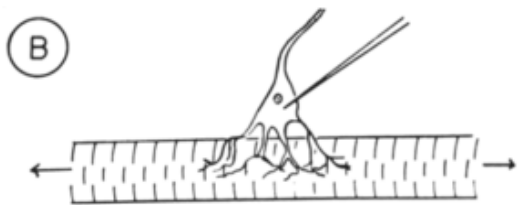


Fig. 1 B of Eyzaguirre and Kuffler (1955a).

Homarus americanus



"Yellow-lobster". Licensed under Creative Commons Attribution-Share Alike 3.0 via Wikimedia Commons.

Mismatch between somatic and axonal AP?

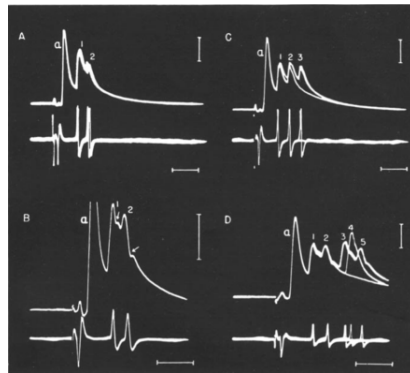


FIG. 13. Simultaneous intra- and extracellular records of grouped discharges in a slow cell. A, intracellular soma record (upper trace) shows superimposed at a 10/sec. stimulation rate components 1 and 2 following the large antidiromic spike (a). The lower trace shows consistently two afferent axon impulses. B, higher amplification, single sweep, shows that in addition to components 1 and 2 there occurs abortive soma activity (arrows), not associated with axon impulses which are only 2 msec. apart. C, superimposed repeated exposures. Component 3 and its associated axon impulse drop out in several sweeps. D, components 1 and 2 are always present while 3 and 5 do not appear on some traces. Component 4 (fainter trace) is seen once or twice in the absence of 3 and 5. Note that small soma potential components (not numbered) may be only 0.5 to 2 msec. apart. Potential calibration, 25 mv. Time, 5 msec.

Fig. 13 of Eyzaguirre and Kuffler (1955b) *J Gen Phys* 39:121.

This is not an invertebrate peculiarity (1)

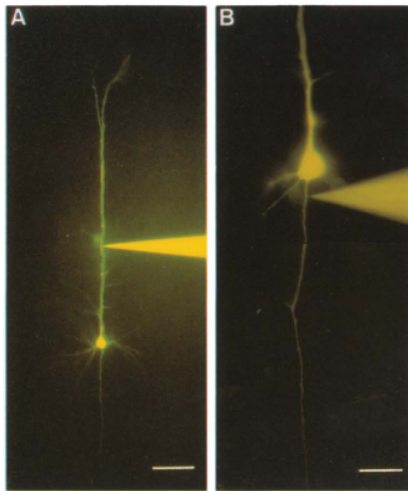


Fig. 7 of Sakmann and Stuart (2009) in *Single-Channel Recording*, edited by B Sakmann and E Neher, Springer

This is not an invertebrate peculiarity (2)

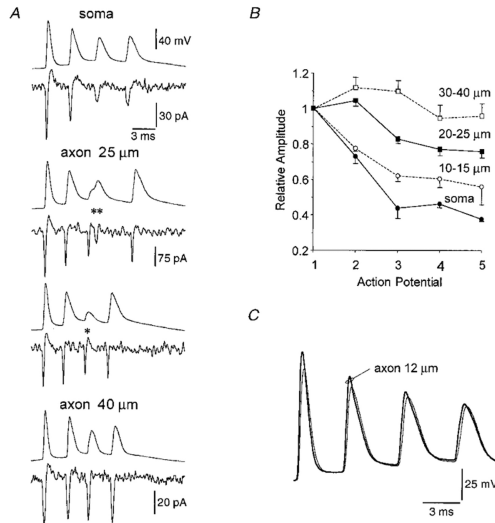


Fig. 5 of Williams and Stuart (1999) *J Physiol* 521:467.

No more than a HH model is required

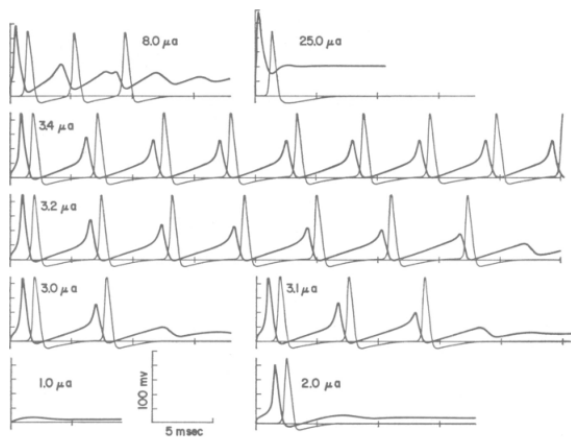


FIGURE 5 Response of the continuous axon to a steady stimulus of various intensities showing time course of the membrane potential V at $x = 0$ (heavy lines) and at $x = 2$ cm (lighter lines).

Fig. 5 of Cooley and Dodge (1966) *Biophys J* 6:583.

A note on slice recording (1)

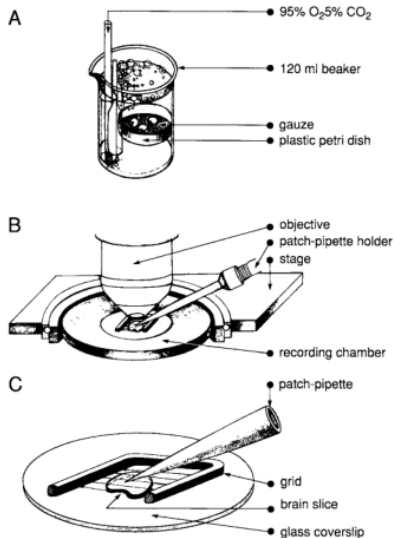


Fig. 1 of Sakmann and Stuart (2009)

A note on slice recording (2)

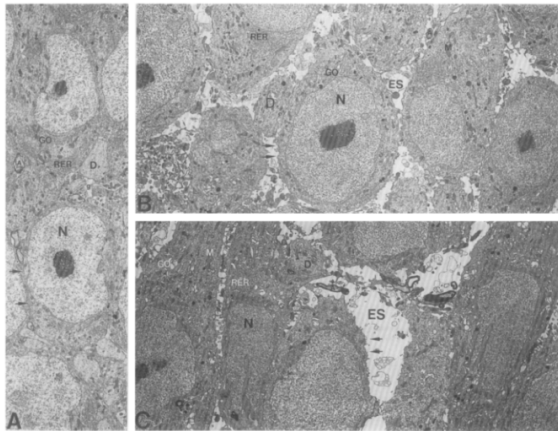


Fig. 2. Electron micrographs of CA1 pyramidal layer cells from the guinea-pig hippocampus. A: brain which was fixed *in situ*. B: from slices prepared using the 45 min zero Ca/10 Mg pre-incubation paradigm. C: from slices prepared in standard buffer only. Cells in (A) and (B) are class I. Cells in (C) are class II and class III. The arrows denote the plasmalemmal regions of the cells. Note the larger apparent extracellular spaces in the slices. Scale: 1 cm = 3 μ m.

Fig. 2 of Aitken et al (1995) *J Neurosci Methods* 59:139.

What happens when the diameter increases?

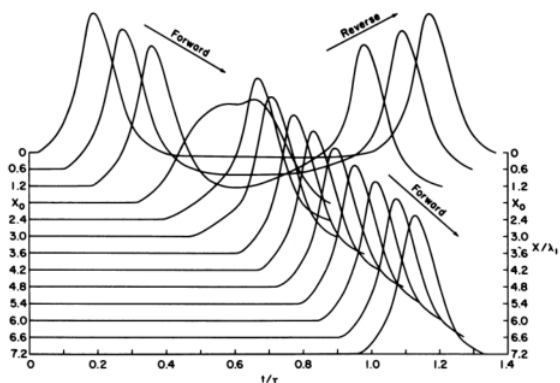


FIGURE 10 Forward and reverse propagation of the action potential in a region of step increase. The action potentials (in the time domain) are shown at successive locations indicated by the vertical scale with X_0 being the point of step increase. In this figure $d_2/d_1 = 2.5$; the kinetic parameters used are shown as set B in Table I.

Numerical model, Fig. 10 of Goldstein and Rall (1974)
Biophys J 14:731.

Reflected AP can happen!

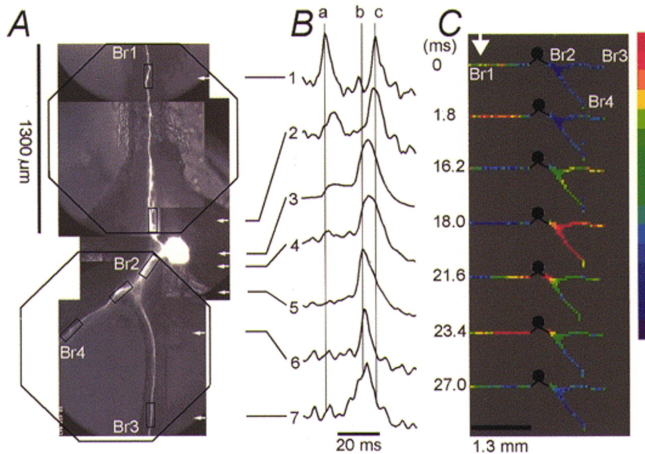


Fig. 5 of Antic et al (2000).

Where are we ?

Ensemble recordings

What is spike sorting?

What do we measure?

A short history of spike sorting

Sorting by eye

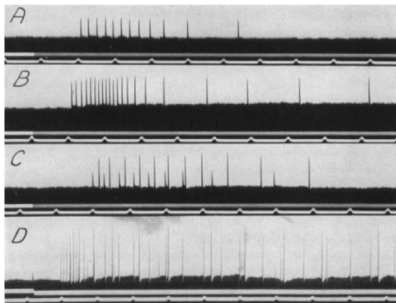


Fig. 4 Action potentials from nerve strands containing several active fibers. A to C) From bundle containing two active fibers. A and B) Stimulation of respective end organs separately. Intensity, 0.1. C) Stimulation of both end organs simultaneously. Intensity, 0.03. D) Record showing discharge in three active fibers. Recording as in figure 2.

As soon as the "the all-or-nothing response of sensory nerve fibres" was established by Adrian and Forbes (1922), neurophysiologists started doing sorting by eye using the spike amplitude as a feature. Fig. 4 of Hartline and Graham (1932) *J Cell Comp Physiol* 1:277. *Limulus polyphemus* recording.

What a *Limulus polyphemus* looks like?



"*Limulus polyphemus* (aq.)" by Hans Hillewaert - Own work.
Licensed under Creative Commons Attribution-Share Alike 4.0
via Wikimedia Commons.

Automatic window discriminator (1963)

FIG. 4. Above, block diagram indicates the mode of operation of the differential amplitude discriminator which is described in full in the text. To the left, below: upper trace shows multi-unit record of thalamic cellular activity. The action potentials of two single units are clearly discernible. Lower trace shows output of DAD when only the larger spike enters and reverses within the potential window. To the right, below: upper trace is same record, but now the potential window has been moved so that only the small spike reverses within it, while the larger one traverses both lower and upper potential levels. Lower trace is DAD output, showing selection of smaller spike.

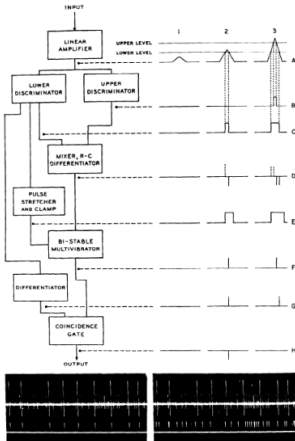


Fig. 4 of Poggio and Mountcastle (1963) *J Neurophys*
26:775. *In vivo* recordings from monkeys thalamic neurons.

Template matching (1964)

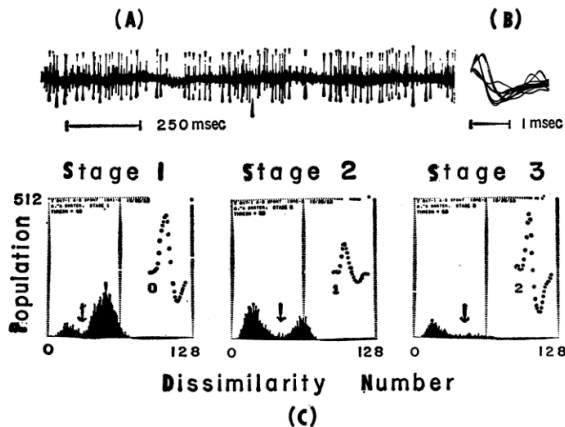


Fig. 1. Action potentials from several adjacent neurons. *A*, Approximately 1.5 seconds of action potential data from several units. *B*, Multiple triggered sweeps of an oscilloscope at high speed to show the three waveforms of action potentials in the data. *C*, Population as a function of dissimilarity number during three stages of the separation (see text).

Fig. 1 of Gerstein and Clark (1964) *Science* 143:1325. Dorsal cochlear nucleus recordings from anesthetized cats.

Dimension reduction and cluster membership (1965)

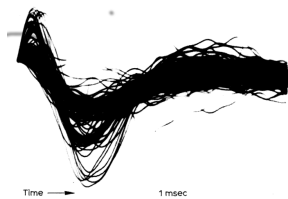


Fig. 1

At least three clearly defined groups of action potentials can be seen in the above photograph.

A fourth group is discernible just under the first peak on the left.

Electroenceph. clin. Neurophysiol., 1965, 17, 192-195



Fig. 2

The computer marks the times at which samples are taken by blanking points on the trace. The two points shown here were quite effective separators of the four groups. The sweep rate is twice that of Fig. 1.

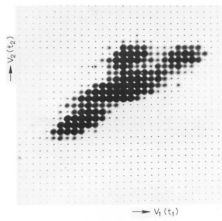


Fig. 1-3 of Simon (1965) *Electroenceph clin Neurophysiol*
18:192.

Superposition resolution (1972)

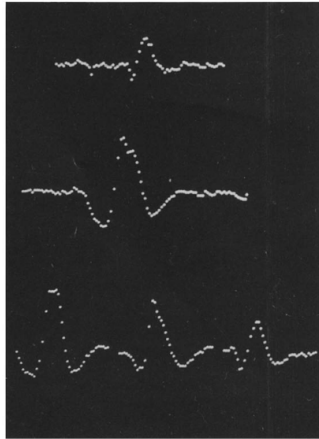
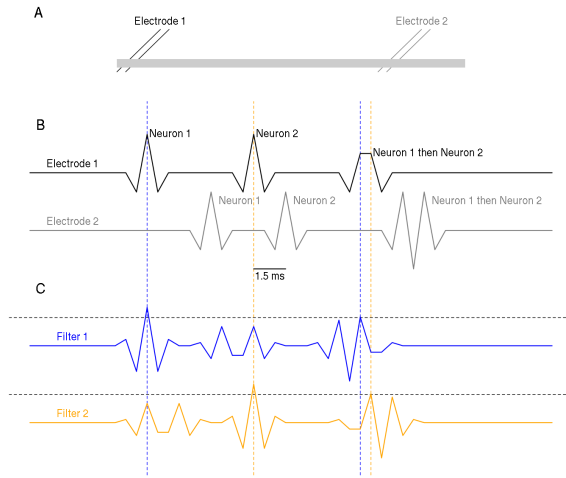


Fig. 3. Photograph of PDP-12 screen showing the display during an interference-potential analysis (all traces stationary and recalled from memory). *Upper trace*: result of subtraction of left template unit from the interference potential (*middle trace*). *Lower trace*: "contemporary" template units.

Fig. 3 of Prochazka et al (1972) *Electroenceph clin Neurophysiol* 32:95.

Multi-channel linear filter: principle (1)



Multi-channel linear filter: principle (2)

You can reconstruct the figure with the following waveforms:

- ▶ **Neuron 1**: electrode 1 (-1,2,1,0,0,0,0,0,0) and electrode 2 (0,0,0,0,0,0,-1,2,-1).
- ▶ **Neuron 2**: electrode 1 (-1,2,1,0,0,0,0,0,0) and electrode 2 (0,0,0,-1,2,-1,0,0,0).

And the following filters:

- ▶ **Neuron 1**: electrode 1 (-1/2,1,1/2,0,0,0,0,0,0) and electrode 2 (0,0,0,0,0,-1/2,1,-1/2).
- ▶ **Neuron 2**: electrode 1 (-1/2,1,1/2,0,0,0,0,0,0) and electrode 2 (0,0,0,-1/2,1,-1/2,0,0,0).

Given signals $E_1(t)$ and $E_2(t)$ on electrode 1 and 2, the output of filter 1 (responding to Neuron 1) is:

$$F_1(t) = -E_1(t-1)/2 + E_1(t) - E_1(t+1)/2 - E_2(t+5)/2 + E_2(t+6) - E_2(t+7)/2.$$

Multi-channel linear filter (1975)

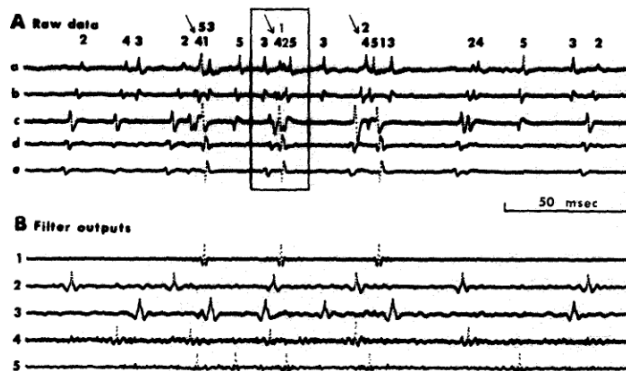


Fig. 2. A: a 200 msec portion of a single burst of neuronal activity from the cardiac ganglion of a spiny lobster (data provided by W. O. Friesen). Activity is monitored at 5 points along the ganglionic trunk with bipolar extracellular electrodes (traces from top to bottom successively more posterior positions). The numbers at the top show the identity of each impulse; they correspond to the numbers in Fig. 1. The portion of the record contained in the box is shown enlarged in Fig. 3. B: output from each of the 5 filters. Fast-rising 'pulses' correspond exactly to occurrences of the unit to which the filter is tuned. Unwanted units produce very little response or 'cross-talk'. Superposition of waveforms from two or more units does not affect filter performance (arrows). Ten similar bursts were analyzed in this run with no errors by the filters.

Fig. 2 of Roberts and Hartline (1975) *Brain Res* 94:141.

Waveform changes during bursts (1973)

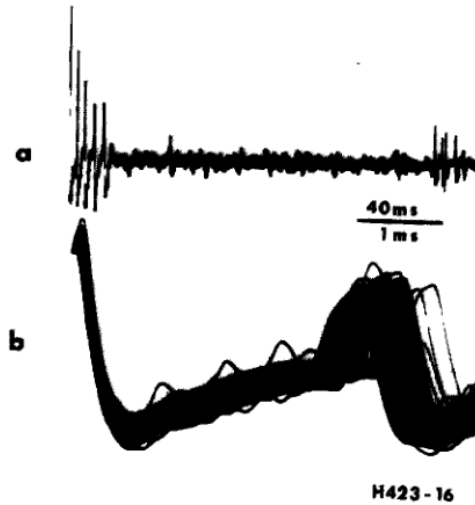


Fig. 2 of Calvin (1972) *Electroenceph clin Neurophysiol* 34:94.

McNaughton, O'Keefe and Barnes solution (1983)

The method described in the present report is based on the fact that the size of the extracellular action potential varies inversely with the distance of the recording electrode from the current generator. In theory, a closely spaced tetrahedral array of recording electrodes with tips sufficiently close together to record signals from overlapping populations of neurons should permit the unique identification of all neuronal spikes which exceed the noise level. This is so since each cell would generate a unique point in the three-dimensional data space whose axes are defined by the spike height ratios of channels 1 and 2, 2 and 3, and 3 and 4. Note, that since the discrimination is based on amplitude ratios, the problem of intrinsic variation in spike amplitude such as occurs during the complex spike burst of hippocampal pyramidal cells is, in principle, solved.

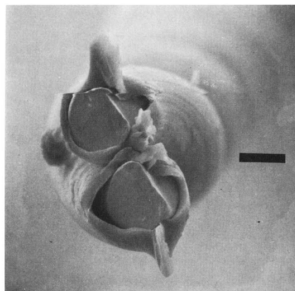


Fig. 1. Scanning electronmicrograph of a 'stereotrode' constructed by twisting together two lengths of 25 μm teflon-insulated wire, and cutting the ends with sharp scissors. Original magnification 240 \times . Calibration bar 20 μm .

Part of the Introduction and Fig. 1 of McNaughton et al
(1983) *J Neurosci Methods* 8:391.

McNaughton, O'Keefe and Barnes solution (1983)

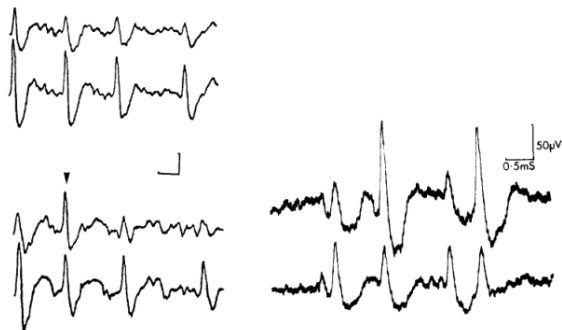


Fig. 2. Two stereotrode records selected from the same data set to illustrate the discrimination of a true complex-spike burst from a single generator (upper pair of traces), from a spurious 'burst' (lower pair of traces) which resembles a complex-spike on the Y channel but clearly contains a spike from a second generator (arrow).

Fig. 3. A second example of spikes which would be indiscriminable using spike height on a single channel, but clearly belong to two different cells when the two-channel amplitude ratio is considered.

Fig. 2 and 3 of McNaughton et al (1983)

McNaughton, O'Keefe and Barnes solution (1983)

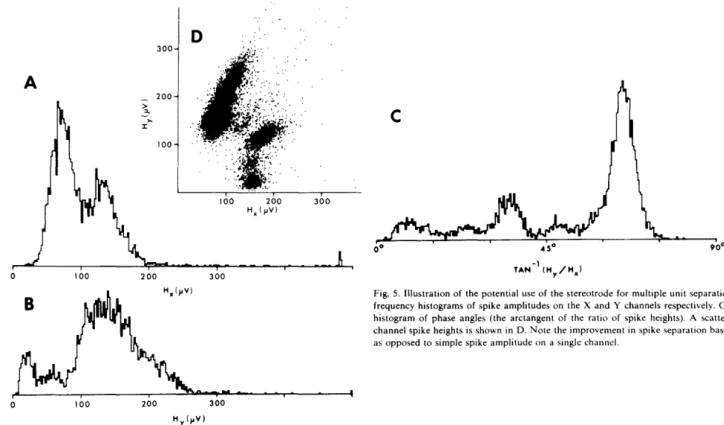


Fig. 5. Illustration of the potential use of the stereotrode for multiple unit separation. A and B show the frequency histograms of spike amplitudes on the X and Y channels respectively. C shows the frequency histogram of phase angles (the arctangent of the ratio of spike heights). A scatter plot of Y versus X channel spike heights is shown in D. Note the improvement in spike separation based on the phase angle as opposed to simple spike amplitude on a single channel.

Fig. 5 of McNaughton et al (1983)

Sampling jitter (1984)

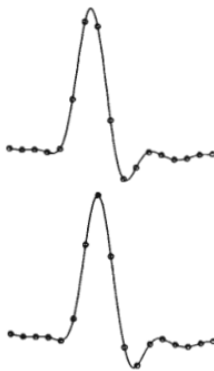


Fig. 1. Two copies of the same waveform, sampled near the Nyquist rate. Sampling at the Nyquist rate only sketches the underlying continuous waveform, and two renditions are apt to appear quite different if the samples are out of phase.

Fig. 1 of McGill and Dorfman (1984) *IEEE Trans Biomed Eng*
31:462. **EMG recordings.**

Sampling jitter correction

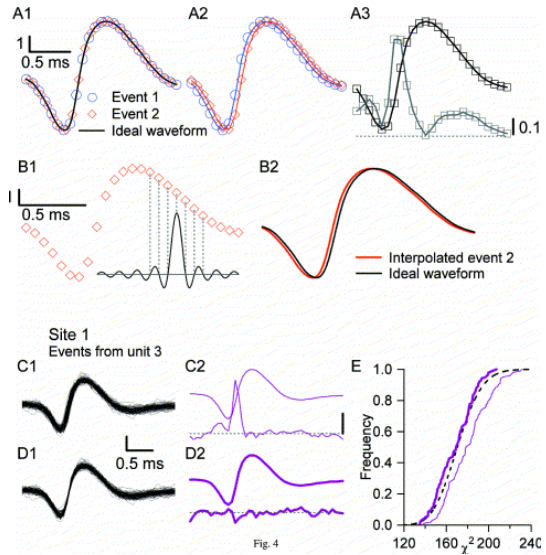
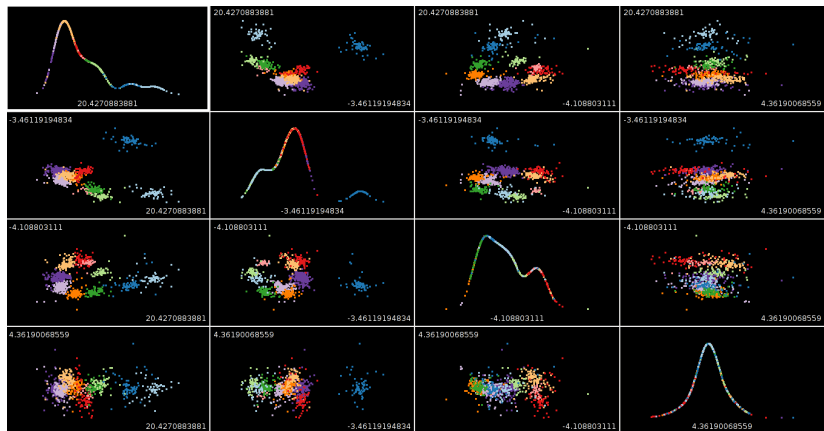


Fig. 4 of Pouzat et al (2002) *J Neurosci Methods* 122:43.

Sophisticated visualization tools (late 80s early 90s)



A scatter plot matrix obtained with GGobi (www.ggobi.org).

Automatic clustering: K-means (1)

Algorithm 14.1 *K-means Clustering.*

1. For a given cluster assignment C , the total cluster variance (14.33) is minimized with respect to $\{m_1, \dots, m_K\}$ yielding the means of the currently assigned clusters (14.32).
2. Given a current set of means $\{m_1, \dots, m_K\}$, (14.33) is minimized by assigning each observation to the closest (current) cluster mean. That is,

$$C(i) = \operatorname{argmin}_{1 \leq k \leq K} \|x_i - m_k\|^2. \quad (14.34)$$

3. Steps 1 and 2 are iterated until the assignments do not change.
-

$$C^* = \min_C \sum_{k=1}^K N_k \sum_{C(i)=k} \|x_i - \bar{x}_k\|^2$$

can be obtained by noting that for any set of observations S

$$\bar{x}_S = \operatorname{argmin}_m \sum_{i \in S} \|x_i - m\|^2. \quad (14.32)$$

Hence we can obtain C^* by solving the enlarged optimization problem

$$\min_{C, \{m_k\}_1^K} \sum_{k=1}^K N_k \sum_{C(i)=k} \|x_i - m_k\|^2. \quad (14.33)$$

This can be minimized by an alternating optimization procedure given in Algorithm 14.1.

Automatic clustering: K-means (2)

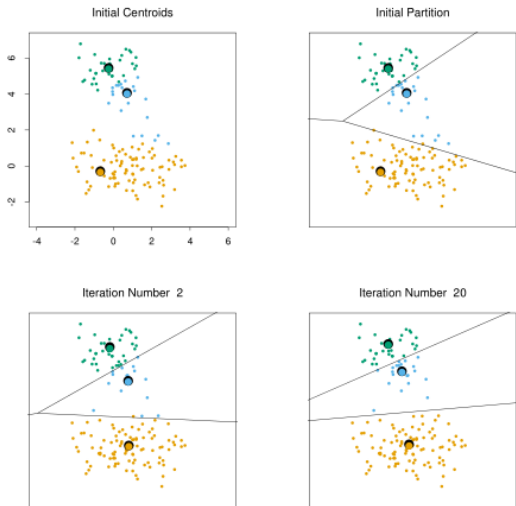


Fig. 14.6 of Hastie et al (2009).

Gaussian Mixture Model (GMM)

GMM can be viewed as "refined" and "softer" version of the K-means. Here an individual observation is assumed to arise from the following procedure, with K components in the mixture:

1. Draw the mixture component $j \in \{1, \dots, K\}$ with probabilities $\{\pi_1, \dots, \pi_K\}$ ($\sum_{i=1}^K \pi_i = 1$).
2. Given j , draw the observation $Y \in \mathbb{R}^p$ from a (multivariate) Gaussian distribution with pdf:

$$\phi_{\mu_j, \Sigma_j}(y) = \frac{1}{(2\pi)^{p/2} |\Sigma_j|^{1/2}} \exp\left(-\frac{1}{2}(y - \mu_j)^T \Sigma_j^{-1} (y - \mu_j)\right).$$

The N observations are assumed to be drawn independently and identically.

The pdf of $y \in \mathbb{R}^p$ can then be written as:

$$p_Y(y) = \sum_{j=1}^K \pi_j \phi_{\mu_j, \Sigma_j}(y).$$

GMM inference: Expectation-Maximization (1)

Let us consider a simple case in dimension 1 with two components. We have:

- ▶ $Y_1 \sim \mathcal{N}(\mu_1, \sigma_1^2)$
- ▶ $Y_2 \sim \mathcal{N}(\mu_2, \sigma_2^2)$
- ▶ $Y = (1 - Z)Y_1 + ZY_2$

where $Z \in \{0, 1\}$ with $\Pr(Z = 1) = \pi$. The density of Y is then:

$$p_Y(y) = (1 - \pi)\phi_{\mu_1, \sigma_1}(y) + \pi\phi_{\mu_2, \sigma_2}(y)$$

and the (log-)likelihood, when an IID sample of size N has been observed, is:

$$l(\pi, \mu_1, \sigma_1, \mu_2, \sigma_2) = \sum_{i=1}^N \ln [(1 - \pi)\phi_{\mu_1, \sigma_1}(y_i) + \pi\phi_{\mu_2, \sigma_2}(y_i)] .$$

GMM inference: Expectation-Maximization (2)

The Expectation-Maximization (EM) algorithm for GMM "augments" the data, doing "as if" the component of origin had been observed, that is as if (Y, Z) instead of simply Y was known. The complete log-likelihood is then:

$$l_0(\pi, \mu_1, \sigma_1, \mu_2, \sigma_2) = \sum_{i=1}^N (1 - z_i) \ln \phi_{\mu_1, \sigma_1}(y_i) + z_i \ln \phi_{\mu_2, \sigma_2}(y_i) + \sum_{i=1}^N (1 - z_i) \ln(1 - \pi) + z_i \ln(\pi).$$

Since the z_i are not known, the EM proceeds in a iterative fashion, by substituting their expected values:

$$\gamma_i = E(Z_i | \pi, \mu_1, \sigma_1, \mu_2, \sigma_2) = \Pr(Z_i = 1 | \pi, \mu_1, \sigma_1, \mu_2, \sigma_2),$$

also called the **responsibility** of the second component for observation i .

GMM inference: Expectation-Maximization (3)

Algorithm 8.1 EM Algorithm for Two-component Gaussian Mixture.

1. Take initial guesses for the parameters $\hat{\mu}_1, \hat{\sigma}_1^2, \hat{\mu}_2, \hat{\sigma}_2^2, \hat{\pi}$ (see text).
2. *Expectation Step:* compute the responsibilities

$$\hat{\gamma}_i = \frac{\hat{\pi}\phi_{\hat{\theta}_2}(y_i)}{(1 - \hat{\pi})\phi_{\hat{\theta}_1}(y_i) + \hat{\pi}\phi_{\hat{\theta}_2}(y_i)}, \quad i = 1, 2, \dots, N. \quad (8.42)$$

3. *Maximization Step:* compute the weighted means and variances:

$$\begin{aligned} \hat{\mu}_1 &= \frac{\sum_{i=1}^N (1 - \hat{\gamma}_i)y_i}{\sum_{i=1}^N (1 - \hat{\gamma}_i)}, & \hat{\sigma}_1^2 &= \frac{\sum_{i=1}^N (1 - \hat{\gamma}_i)(y_i - \hat{\mu}_1)^2}{\sum_{i=1}^N (1 - \hat{\gamma}_i)}, \\ \hat{\mu}_2 &= \frac{\sum_{i=1}^N \hat{\gamma}_i y_i}{\sum_{i=1}^N \hat{\gamma}_i}, & \hat{\sigma}_2^2 &= \frac{\sum_{i=1}^N \hat{\gamma}_i (y_i - \hat{\mu}_2)^2}{\sum_{i=1}^N \hat{\gamma}_i}, \end{aligned}$$

and the mixing probability $\hat{\pi} = \sum_{i=1}^N \hat{\gamma}_i / N$.

4. Iterate steps 2 and 3 until convergence.
-

Hastie et al (2009) p 275.

Automatic choice of K

The number of components can be automatically chosen by minimizing a penalized likelihood with **Akaike's Information Criterion** (AIC):

$$K = \arg \min_k -2I(\hat{\theta}_k) + 2d(k),$$

where $\hat{\theta}_k$ stands for maximum likelihood estimator of the set of model parameters and $d(k)$ stands for the dimension (number of parameters) of the model.

Schwarz's **Bayesian Information Criterion** (BIC) tends to work better:

$$K = \arg \min_k -2I(\hat{\theta}_k) + \ln(N)d(k),$$

where N is the sample size.

See Chap. 7 of Hastie et al (2009) for more criteria and discussion.

That's all for today!

Thank you for listening!